Dimethylalkoxygallanes: Monomeric versus Dimeric Gas-Phase Structures

Caroline E. Knapp,[†] Derek A. Wann,*[,‡] Andrzej Bil,*[,§] Julien T. Schirlin,[‡] Heather E. Robertson,[‡] Paul F. McMillan,[†] David W. H. Rankin,[‡] and Claire J. Carmalt*[,†]

[†]Materials Chemistry Centre, Department of Chemistry, University College London, 20 Gordon Street, London, U.K. WC1H 0AJ
[‡]School of Chemistry, University of Edinburgh, West Mains Road, Edinburgh, U.K. EH9 3JJ
[§]Faculty of Chemistry, University of Wrocław, Joliot-Curie 14, PL-50-383 Wrocław, Poland

Ⓢ *Supporting Information*

ABSTRACT: The molecular structures of the vapors produced on heating dimethylalkoxygallanes of the type $[Me_2Ga(OR)]_2$ have been determined by gas electron diffraction and ab initio molecular orbital calculations. In the solid state $[Me_2Ga(OCH_2CH_2NMe_2)]_2$ (**1**) and $[Me_2Ga(OCH_2CH_2OMe)]_2$ (**2**) adopt dimeric structures, although only the monomeric forms $[Me_2Ga(OCH_2CH_2NMe_2)]$ (**1a**) and $[Me_2Ga(OCH_2CH_2OMe)]$ (**2a**) were observed in the gas phase. For comparison the structure of the vapor produced on heating $[Me_2Ga(O^tBu)]_2$ (**3**) was also studied by gas electron diffraction. In contrast to **1** and **2**, compound **3** is dimeric in the gas phase, as well as in the solid state. The gas-phase structures of **1a** and **2a** exhibit five-membered rings formed by a dative bond between Ga and the donor atom (N or O) from the donor-functionalized alkoxide. In **3** there is no possibility of a monomeric structure being stabilized by the formation of such a dative bond since only a monofunctional alkoxide is present in the molecule.

solid → gas

solid and gas are same
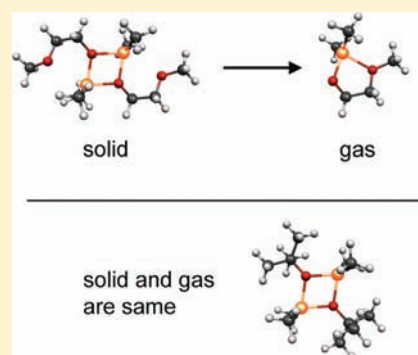
■ INTRODUCTION

Diorganoalkoxygallanes of the type $[R'_2Ga(OR)]_n$ have been known for many years, and their syntheses, structures and reactivities have been the subject of recent detailed reviews.[1,2] Many of the gallium mono(alkoxides) have been structurally characterized and were found to be either monomeric or dimeric via oxygen bridges. Which structure is adopted is governed by the electronic and steric properties of both the alkoxide and alkyl/aryl ligands.

The outer electronic configuration of gallium is $[Ar]3d^{10}4s^24p^1$, which leads to a typical formal oxidation state of +3. However, the three electron pairs that can be formed by the valence electrons on Ga and those on other atoms do not completely fill the valence space. This, therefore, allows for the formation of an extra dative bond with both electrons coming from the ligand. In this way, the gallium atom in a simple inorganic compound tends to form a tetrahedral unit, while an octahedral coordination pattern is also common.

Diorganoalkoxygallanes were first reported nearly 60 years ago and are usually synthesized via the reaction of GaR'_3 and an alcohol (ROH).[3] For example, the reaction of $GaMe_3$ with ^tBuOH results in the formation of dimeric $[Me_2Ga(O^tBu)]_2$.[4] In general, gallium alkoxides form dimers, trimers, and tetramers via the formation of Ga–O bridging bonds.[2,4]

Interest in these and related gallium alkoxide compounds stems from their uses as precursors to gallium oxide (Ga_2O_3) thin films by low-pressure chemical vapor deposition (LPCVD)[5−7] and aerosol-assisted CVD.[8−13] Often it is necessary in CVD applications to tailor the properties of the precursor to optimize process parameters such as decomposition temperature, film purity, and uniformity and evaporation temperature. It has previously been shown that the use of donor-functionalized alkoxides, for example, $OCH_2CH_2NMe_2$ or OCH_2CH_2OMe, in place of simple alkoxide groups, such as OMe or O^tBu, can result in the formation of precursors with enhanced CVD performance and improved physical properties (volatility, solubility, thermal stability).[5,8,13] Although gallium and indium oxides are of interest for transparent conducting oxide (TCO)[14,15] and gas sensing[16,17] applications, little information is available on the gas-phase structures of typical precursors employed for film growth.[18] An understanding of the behaviors and structures of CVD precursors in the gas phase would provide important information about the decomposition processes central to CVD[19,20] as well as potentially leading to improvements in precursor design and film growth.[21−23]

Herein we describe the structural characterizations of the monomeric forms of **1** and **2** in the gas phase using a combined electron diffraction and computational approach. We also present the structure of $[Me_2Ga(O^tBu)]_2$, **3**, which retains its dimeric structure in the gas phase. This difference in behavior gives us an insight into the driving force behind the transition from dimer to monomer for **1** and **2**, potentially a key step in the decomposition process during CVD. A communication of part of this work relating to the gas-phase structure of the monomeric form of **1** has appeared.[18]

■ EXPERIMENTAL SECTION

General Procedures. All manipulations were performed under a dry, oxygen-free dinitrogen atmosphere using standard Schlenk techniques or in an Mbraun glovebox. All solvents used were stored in alumina columns and dried with anhydrous engineering equipment, reducing the water concentration to 5−10 ppm. All chemicals were supplied by SAFC Hitech or procured commercially from Aldrich and used without further purification, with the exception of alcohols, which were further distilled and degassed and stored over molecular sieves. Analytical data were obtained at UCL.

Physical Measurements. A Bruker AMX400 spectrometer was used to record all ^1H and ^{13}C NMR spectra, operating at 299.87 and 400.12 MHz, respectively. All spectra were recorded using C_6D_6, which was dried and degassed over molecular sieves prior to use; ^1H and ^{13}C chemical shifts are reported relative to $SiMe_4$. All IR spectra were recorded using a Shimadzu FTIR-8200 spectrometer, operating in the region of 4000−400 cm^{-1}. The IR samples were prepared using Nujol. The mass spectra were obtained from toluene solutions of 1−3 using a Micromass 70-SE spectrometer using chemical ionization (CI) with methane reagent gas. The elemental analysis was carried out using a CE-440 Elemental Analyzer (Exeter Analytical Inc.).

Syntheses. Samples of $[Me_2Ga(OCH_2CH_2NMe_2)]_2$ (**1**) and $[Me_2Ga(OCH_2CH_2OMe)]_2$ (**2**) were prepared by the reaction of $GaMe_3$ in toluene and $HOCH_2CH_2X$ (X = NMe_2 or OMe) using slightly modified versions of the route previously published.[24,25] $[Me_2Ga(O^tBu)]_2$ (**3**) was similarly prepared from the reaction of Me_3Ga with *tert*-butanol in toluene.[26]

[Me₂Ga(OCH₂CH₂NMe₂)]₂ (1). Anal. Calcd for $C_{12}H_{32}Ga_2O_2N_2$: C, 38.5; H, 9.63; N, 7.48 (%). Found: C, 38.38; H, 9.32; N, 7.13 (%). ^1H NMR δ/ppm (C_6D_6): −0.20 (s, GaCH_3, 6H), 1.98 (s, NCH_3, 6H), 2.01 (t, OCH$_2$CH_2N, 2H), 3.49 (t, OCH_2CH$_2$N, 2H). $^{13}C\{^1H\}$NMR δ/ppm (C_6D_6): 5.2 (GaCH_3), 45.2 (NCH_3), 59.1 (OCH$_2$CH_2N), 61.7 (OCH_2). FTIR (cm^{-1}): 2924 vs, 2789 w, 2719 w, 2700 w, 1666 s, 1420 m, 1356 m, 1273 s, 1233 w, 1187 m, 1165 w, 1036 m, 1000 m, 954 m, 932 m, 894 m, 786 m, 629 m, 552 m, 504 m, 430 m. Mass spec. (CI): (m/z) 374 $[M]_2$, 359 $[M]_2$ minus Me, 286 $[M]_2$ minus ($OCH_2CH_2NMe_2$), 172 MeGa($OCH_2CH_2NMe_2$), 99 (Me_2Ga).

[Me₂Ga(OCH₂CH₂OMe)]₂ (2). Anal. Calcd for $C_{10}H_{26}Ga_2O_4$: C, 34.48; H, 7.47; N, 0.00 (%). Found: C, 34.21; H, 7.01; N 0.00 (%). ^1H NMR δ/ppm (C_6D_6): −0.21 (s, GaCH_3, 6H), 2.89 (s, OCH_3, 3H), 3.44 (t, OCH$_2$CH_2OCH$_3$, 2H), 3.79 (t, OCH_2CH$_2$OCH$_3$, 2H). $^{13}C\{^1H\}$NMR δ/ppm (C_6D_6): 5.1 (GaCH_3), 59.1 (OCH_3), 62.9 (OCH$_2$CH_2OCH$_3$), 72.8 (OCH_2CH$_2$OCH$_3$). FTIR (cm^{-1}): 2935 s, 2865 m, 2726 m, 2373 m, 2152 m, 2046 m, 1975 m, 1568 s, 1456 s, 1418 m, 1394 m, 1362 m, 1261 s, 1237 s, 1198 s, 1127 s, 1081 s, 1025 s, 960 s, 908 s, 849 s, 801 vs, 654 vs. Mass spec. (CI): (m/z) 348 $[M]_2$, 273 $[M]_2$ minus (OCH_2CH_2OMe), 174 Me₂Ga(OCH_2CH_2OMe), 99 (Me_2Ga).

[Me₂Ga(O^tBu)]₂ (3). Anal. Calcd for $C_{12}H_{30}Ga_2O_2$: C, 41.86; H, 8.72; N, 0.00 (%). Found: C, 41.56; H, 8.31; N 0.00 (%). ^1H NMR δ/ppm (C_6D_6): 0.01 (s, GaCH_3, 6H), 1.12 (s, C(CH_3)$_3$, 9H),. $^{13}C\{^1H\}$ NMR δ/ppm (C_6D_6): 73.0 (C(CH$_3$)$_3$), 32.3 (C(CH_3)$_3$), −1.35 (GaCH_3). Mass spec. (CI): (m/z) 344 $[M]_2$, 287 $[M]_2$ minus C(CH$_3$)$_3$, 215 $[M]_2$ minus (CH$_3$)$_3$ minus Me, 172 $[M]$, 157 [MeGa(O^{t}Bu)], 84 MeGa, 57 C(CH$_3$)$_3$. FTIR (cm^{-1}): 2934 vs, 2724 w, 2716 w, 2700 w, 1656 s, 1410 m, 1393 m, 1262 s, 1234 w, 1188 m, 1129 w, 1066 m, 1000 m, 955 m, 930 m, 890 m, 630 m, 552 m.

Computational Methods. All molecular orbital calculations were carried out using the resources provided by the NSCCS[27] running the Gaussian 03 suite of programs,[28] for both monomer and dimer species of 1−3.

For each of the molecules studied geometry optimizations were performed at the Hartree−Fock level with the 3-21G* basis set[29] on all atoms followed by the 6-31G* basis set.[30] Frequency calculations were also performed at this level to ensure that the calculated structures represented minima on the potential-energy surface. Optimizations were then performed using MP2 theory[31] to account for electron correlation. These MP2 calculations included all electrons in the valence shell and were carried out using the 6-311+G* basis set on all atoms.[32]

The program SHRINK[33] was used with harmonic force constants calculated at the B3LYP/6-311+G* level[32,34] to produce sets of starting values for amplitudes of vibration and curvilinear distance corrections for use in each of the Gas Electron Diffraction (GED) refinement undertaken. The same level of calculations were used to obtain other data necessary for the thermochemical analyses of the relative stabilities of the monomeric and dimeric forms of 1, 2, and 3.

The nature of the bonding in selected molecules was also analyzed using topological methods, which are based on the properties of a given scalar field. The Atoms in Molecules (AIM) approach proposed by Bader[35] is concerned with electron density and allows chemical bonds to be identified and quantitatively described. A bond can be characterized by the value of the electron density (ρ) and the gradient or Laplacian of the electron density ($\nabla \rho$) calculated at the bond critical point, as well as by the delocalization index, which can be interpreted as a bond order. A negative value of $\nabla \rho$ at the bond critical point characterizes a bond as shared (the electron density is locally concentrated), whereas a positive value defines a closed-shell type of interaction (the electron density is locally depleted). From a chemical point of view the former case, together with a large value of electron density, is typical of a covalent bond, while the latter is characteristic of ionic or hydrogen bonds, where the bonding is driven by electrostatic interactions.[36] The topological analyses of the calculated electron densities were performed using the AIMA11 software package.[37]

Another topological method used is called Electron Localization Function (ELF), and it allows so-called disjoint basins to be defined and characterized.[38] These can then be interpreted as atomic cores, and bonded or free electron pairs,[39] each of which can help us to understand subtleties in molecular structure. The function in question ranges from 0 to 1; in regions with a higher value, electrons with parallel spins tend to be far from one another.

The wave functions necessary to produce electron density and electron localization functions have been calculated using the MP2 method coupled to the 6-311+G* basis set. Topological properties of these fields have been analyzed using TopMod software.[40]

Gas Electron Diffraction (GED). Data were collected from samples of 1, 2, and 3 using the Edinburgh GED apparatus,[41] using an accelerating voltage of 40 kV, resulting in an electron wavelength of approximately 0.06 Å. It is normal practice to record the scattering intensities on Kodak Electron Image films at two different nozzle-to-film distances, to maximize the scattering angle through which data are collected. For 1 and 3 this was possible, but for 2 the increase in temperature that was required to volatilize the sample for the shorter nozzle-to-film distance caused the sample to degrade. For this reason only data collected at the longer nozzle-to-film distance were used. The temperatures to which the samples and nozzles were heated are given in Supporting Information, Table S1.

That any data were collected for these samples, which decompose at relatively low temperatures compared to the vapor pressures required for the GED experiments, was possible only by using a new slit nozzle (Figure 1).


Figure 1. Photograph of an aluminum high-temperature slit nozzle.

Made of aluminum with a slit 5 mm long and approximately 0.5 mm wide, the nozzle was simply made by squeezing a tube of aluminum

3325

dx.doi.org/10.1021/ic202775x | *Inorg. Chem.* 2012, 51, 3324−3331

over an inserted former, which was then retracted. To use the nozzle it is carefully aligned, with the longer orifice dimension parallel to the electron beam. Once this has been done it allows for an increase in the amount of gas entering the collision zone, as the cross-sectional area is about ten times greater than with a conventional nozzle. Extensive simulations were performed before using the nozzle. These demonstrated that using a 5 mm slit nozzle did not adversely affect the data, while longer slits resulted in abnormalities in the magnitudes of the amplitudes of vibration. Test experiments were performed collecting data using the slit nozzle and a conventional nozzle for benzene, acetone, and CO_2.[42] Refinements using the data from the slit nozzle showed no significant differences when compared to refinements performed with data collected using the conventional nozzle. It was subsequently found that the sample temperature can be reduced by around 40 °C and still give an exposure similar to that obtained using a traditional circular-orifice nozzle at the higher temperature.

The data collection also made use of the sample vessel shown in Figure 2a. The use of this ampule, which is heated using hot air from
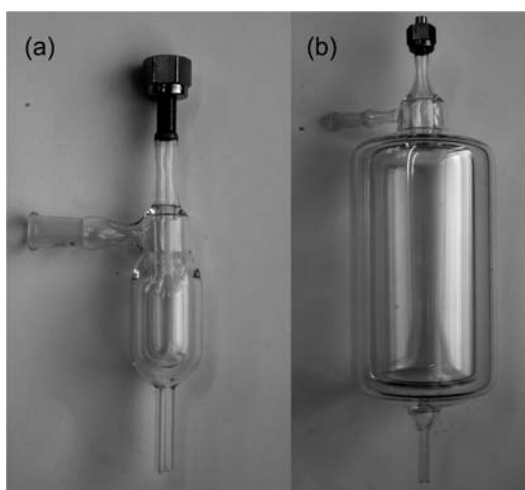
Figure 2. Photographs of (a) the heated ampule used in the present work, and (b) the heated reservoir designed using the same principles.

an inline heater, allows for a more uniform distribution of heat than was commonly achieved using electrical heating tapes. The design of the inner ampule surrounded by a jacket of air was adapted from a design for a heated reservoir.[42] This reservoir, shown in Figure 2b, has an internal volume of approximately 500 cm³, and was designed for use

with samples, usually solids, with low rates of vaporization. It is heated using hot air as for the smaller ampule, albeit with extra insulation in the form of glass wool around the outside of the vessel. At equilibrium there would be sufficient sample in the gas phase for one diffraction pattern to be recorded. Glass-to-metal seals are used in conjunction with Swagelok components to attach these vessels to the diffractometer inlet. The larger reservoir [Figure 2b; approximately 25 cm in length] requires extra support in the form of a clamp stand, whereas the heated ampule [Figure 2a; 10 cm long) can support its own weight.

The data collected for samples of each of **1−3** were scanned using an Epson Expression 1680 Pro flatbed scanner as described elsewhere.[43] The data-reduction processes and the least-squares refinements were carried out using the ed@ed v3.0 program[44] with the scattering factors of Ross et al.[45] The weighting points for the off-diagonal weight matrices, correlation parameters and scale factors for all camera distances for **1−3** are given in Supporting Information, Table S1.

■ RESULTS AND DISCUSSION

The dimethylalkoxygallanes, $[Me_2Ga(OR)]_2$ (R = $CH_2CH_2NMe_2$ **1**; CH_2CH_2OMe **2**; ^tBu **3**), were prepared by the reactions between $GaMe_3$ and ROH using slightly modified versions of literature routes (Scheme 1). Spectroscopic and analytical data for **1−3** confirmed that the samples were pure within the sensitivity of the spectrometers. The crystal structures of **1** and **2** have been reported previously and showed that these complexes adopt dimeric structures in the solid state with planar Ga_2O_2 rings.[24,25] Compound **3** is also dimeric in the solid state. In the FTIR spectra of **1−3**, Ga_2O_2 ring modes were observed at ~650 cm⁻¹, consistent with the dimeric structure. Compounds **1−3** adopt dimeric structures in the solution phase, as indicated by the mass spectroscopy performed in toluene solution. Compounds **1** and **2** have a dative ligand-gallium interaction in solution, as they do in the solid state. This is confirmed by comparing the proton resonances of the alkoxide ligands in **1** and **2** to the relevant free ligand. Thus, in the ¹H NMR spectra of **1** and **2** downfield shifts in the resonances of protons positioned α to the donor heteroatoms are observed.

At the point in this work when the GED refinements for **1** and **2** were performed it was unclear whether we would expect to see monomeric or dimeric species in the gas phase, or indeed both. Ab initio molecular orbital calculations were therefore performed for both the monomeric and dimeric forms of $[Me_2Ga(OCH_2CH_2NMe_2)]_n$ (**1a**, n = 1; **1**, n = 2) and

Scheme 1
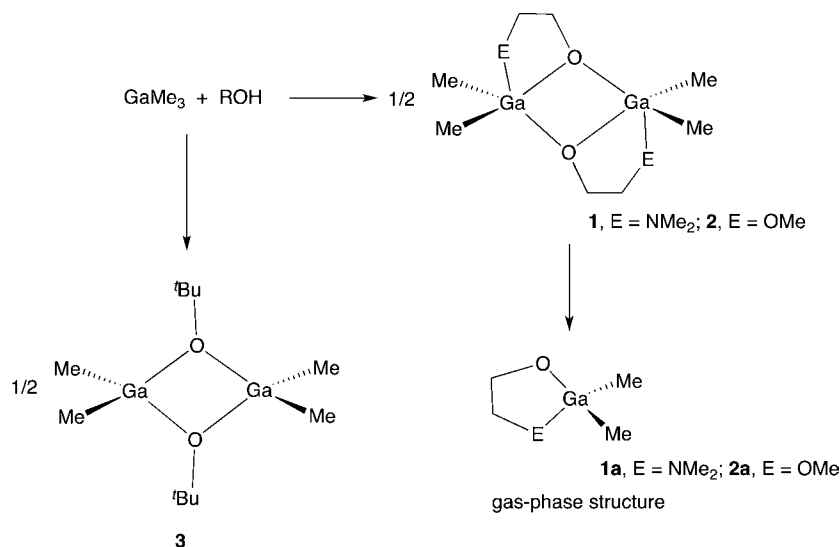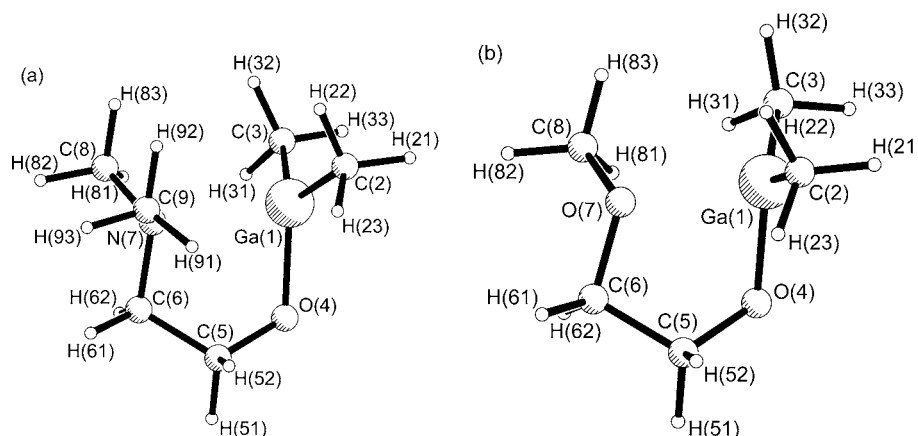
Figure 3. Molecular structures of the monomeric species (a) [Me$_2$Ga(OCH$_2$CH$_2$NMe$_2$)] (**1a**) and (b) [Me$_2$Ga(OCH$_2$CH$_2$OMe)] (**2a**), including atom numbering.

Table 1. Selected Calculated Parameters and GED-Refined Parameters for [Me$_2$Ga(OCH$_2$CH$_2$NMe$_2$)] (1a) and [Me$_2$Ga(OCH$_2$CH$_2$OMe)] (2a)^a

	1a		2a	
	GED (r_{h1})	MP2(full)/6-311+G*	GED (r_{h1})	MP2(full)/6-311+G*
rGa−O(4)	1.906(4)	1.878	1.865(10)	1.866
rGa−C(2)	2.006(2)	1.975	1.971(6)	1.964
rGa−C(3)	2.006(2)	1.972	1.971(6)	1.965
rO(4)−C(5)	1.415(5)	1.397	1.437(7)	1.400
rC(5)−C(6)	1.545(5)	1.529	1.552(8)	1.520
rC(6)−N/O(7)	1.500(4)	1.485	1.476(7)	1.442
rN/O(7)−C(8)	1.488(4)	1.472	1.461(7)	1.427
rN(7)−C(9)	1.490(4)	1.474		
rGa···N/O(7)	2.332(11)	2.168	2.160(20)	2.183
∠O(4)−Ga−C(2)	115.3(8)	114.8	112.2(19)	115.8
∠O(4)−Ga−C(3)	112.8(8)	112.3	108.9(20)	112.7
∠Ga−O(4)−C(5)	116.2(12)	112.5	114.3(9)	111.4
∠O(4)−C(5)−C(6)	110.9(9)	109.6	108.4(11)	109.4
∠C(5)−C(6)−N/O(7)	109.7(9)	109.2	104.4(11)	105.7
∠C(6)−N/O(7)−C(8)	110.7(7)	111.0	112.3(12)	113.5
∠C(6)−N(7)−C(9)	110.3(7)	110.6		
ϕGa−O(4)−C(5)−C(6)	43.0(19)	39.4	54.4(26)	50.2
ϕO(4)−C(5)−C(6)−N/O(7)	−48.1(25)	−52.9	−36.3(38)	−54.1

^{a}Distances (r) are in Å and angles (∠) and dihedral angles (ϕ) are in degrees. See Figure 3 for atom numbering.

[Me$_2$Ga(OCH$_2$CH$_2$OMe)]$_n$ (**2a**, n = 1; **2**, n = 2). It was anticipated that several possible conformers of each structure might exist. Calculations for the dimers **1** and **2** indicated that in isolation they would have structures similar to those in the solid state. The possibilities of dimeric structures with both C_2 and C_i point-group symmetries were considered, and it was calculated that for **1** the only structure representing a minimum had C_2 symmetry. For **2** both the C_2 and C_i structures were minima, and that with C_2 symmetry was slightly lower in energy. For each of the monomer structures **1a** and **2a**, the possibility of closed-ring structures [as shown in Figures 3a and b] as well as open-chain conformers was considered. Selected parameters [MP2(full)/6-311+G*] relating to the C_1-symmetric closed-ring structures of **1a** and **2a** are given in Table 1.

For **3** only geometry optimizations of the dimeric form were performed, with each of the following symmetries imposed: C_s, C_i, C_{2h}, and D_{2h}. The C_{2h} structure (shown in Figure 4) was the only potential minimum to be found. Some parameters calculated at the MP2(full)/6-311+G* level are given in Table 2.

The gas electron diffraction studies of **1−3** were performed by heating the samples under the conditions described in Supporting Information, Table S1. For **1** and **2** the structures derived from the GED data were initially compared with theoretical data representing both monomer and dimer species. It became obvious that the fits to the monomers (see Figure 3) were far superior and so geometric models were written describing the structures of **1a** and **2a** in terms of bond lengths, bond angles and dihedral angles. Detailed descriptions of both models, as well as tables showing all parameters used, are given in Supporting Information (Table S2 for **1a** and Table S3 for **2a**). For **3** it was obvious from the GED data that a dimeric structure (see Figure 4) gave a much better fit. As the only minimum structure on the potential-energy surface was found to have C_{2h} symmetry, the model was written accordingly. Again a detailed description of the model is given in Supporting Information, with all parameters shown in Supporting Information, Table S4. The structure is slightly pyramidal at O(2) and O(8), with the sum of the angles totaling 356.9°.
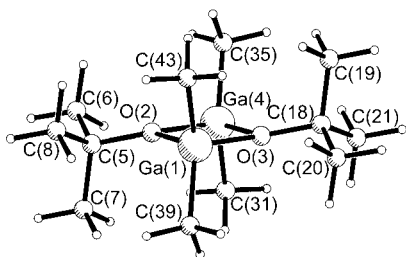
Figure 4. Molecular structure (including atom numbering) of [Me₂Ga-(OᵗBu)]₂ (**3**) with C_{2h} symmetry. Hydrogen-atom labels have been omitted for clarity.

Table 2. GED-Refined Parameters and Highest Level Calculated Parameters for C_{2h}-Symmetric [Me₂Ga(OᵗBu)]₂ (3)[a]

	3	
	GED (r_{h1})	MP2(full)/6-311+G*
rGa−O	1.979(2)	1.970
rGa−C	1.965(3)	1.968
rC−O	1.441(5)	1.438
rC(5)−C(6)	1.539(3)	1.524
rC(5)−C(7)	1.537(4)	1.525
∠Ga−O−Ga	98.5(2)	101.1
∠O−Ga−O	81.5(2)	78.9
∠O−C(5)−C(6)	108.0(5)	107.7
∠O−C(5)−C(7)	110.2(6)	109.8
∠C(31)−Ga−C(35)	122.2(16)	127.4
ϕC(31)−Ga(4)−Ga(1)−O(3)	89.6(31)	87.7

[a]Distances (r) are in Å and angles (∠) and dihedral angles (ϕ) are in degrees. See Figure 4 for atom numbering.

Gibbs free energies, calculated at the B3LYP/6-311+G* level, indicate that the dimeric forms are stable at low temperatures (see Supporting Information, Figure S1). However, under the conditions of high temperature and low pressure, the dimeric forms tend to dissociate. Both the enthalpies and entropies of dimer formation were negative for all temperatures investigated. The fact that the entropy of a system consisting of monomer units must always be larger than that composed of dimers explains why dimers tend to dissociate at higher temperatures. Density functional theory (DFT) calculations cannot, however, provide sufficiently accurate data to predict precisely the range of temperatures where monomeric or dimeric forms are stable. The results of our calculations do indicate that [Me₂Ga-(OCH₂CH₂NMe₂)]₂ (**1**) can dissociate relatively easily, whereas much higher temperatures are necessary for dissociation of [Me₂-Ga(OᵗBu)]₂ (**3**), in agreement with our experimental findings. The calculations also show that the units forming the dimer [Me₂Ga(OCH₂CH₂OMe)]₂ (**2**) are bound more strongly than in **1**, but not as strongly as in **3**. On account of limitations of the model used to calculate the Gibbs free energy, the plot of ΔG for **2** does not allow us to predict with confidence which form should be present at experimental conditions.

For each of **1a**, **2a**, and **3** all independent geometric parameters were refined by least-squares. Some of the more important experimental parameters are listed in Tables 1 and 2 along with their calculated equivalents. Restraints were applied, using the SARACEN method,[46] to parameters that could otherwise not be refined (see Supporting Information, Tables S2−S4). These restraints were based on values calculated at the MP2(full)/6-311+G* level and the uncertainties were derived

from the changes in value of each parameter during the series of calculations that were performed. Additionally, in the case of **1a** 15 amplitudes or groups of amplitudes of vibration were refined (three with SARACEN restraints), for **2a** four groups of amplitudes were refined (two with restraints), and for **3** seven were refined (two with restraints). (See Supporting Information, Table S5−S7 for lists of amplitudes of vibration and curvilinear distance corrections for **1a**, **2a** and **3**, respectively.) The least-squares correlation matrices for the GED refinements of **1a**, **2a**, and **3** are given in Supporting Information, Tables S8−S10, respectively, and coordinates for the final GED structures and for the highest level calculated structure are listed in Supporting Information, Tables S11−S16. The fits of the theoretical models (monomers only for **1a** and **2a**; dimer only for **3**) to the experimental data were good, with $R_G = 0.094$ ($R_D = 0.069$) for **1a**, $R_G = 0.081$ ($R_D = 0.075$) for **2a**, and $R_G = 0.071$ ($R_D = 0.099$) for **3**. These fits can be visualized using the radial-distribution curves in Figure 5, which show the experimental curves and the experimental-minus-theoretical
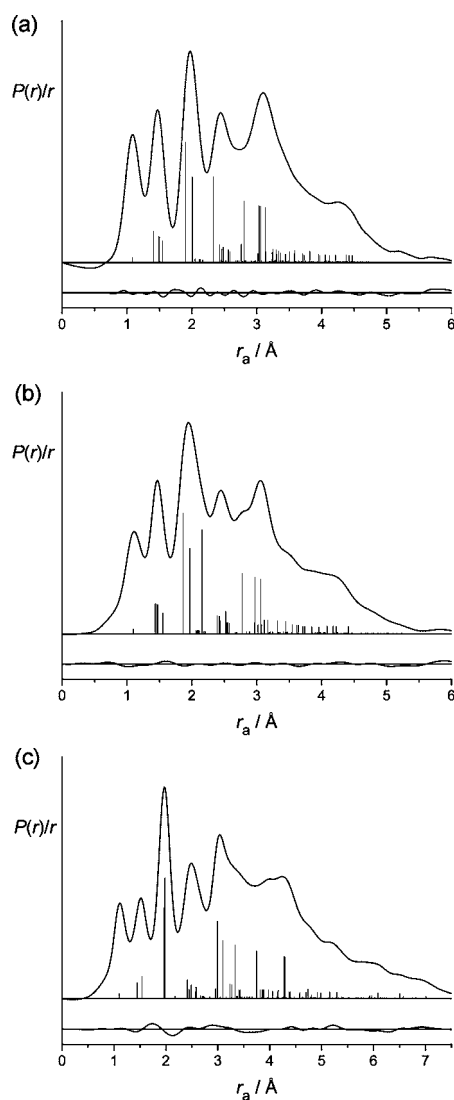
Figure 5. Experimental radial distribution and difference (experimental minus theoretical) curves for the GED refinements of (a) [Me₂Ga(OCH₂CH₂NMe₂)] (**1a**), (b) [Me₂Ga(OCH₂CH₂OMe)] (**2a**), and (c) [Me₂Ga(OᵗBu)]₂ (**3**). Before Fourier transform the data were multiplied by $s\cdot\exp(-0.00002s^2)/(Z_{Ga} - f_{Ga})(Z_C - f_C)$.

difference curves. The molecular scattering intensity curves are shown in Supporting Information, Figures S2−S4. If there had been a proportion of the dimeric forms of **1** and **2** present in the gas-phase samples there would have been evidence for interatomic interactions at distances longer than about 6 Å.

The GED structures of $[Me_2Ga(OCH_2CH_2NMe_2)]$ (**1a**) and $[Me_2Ga(OCH_2CH_2OMe)]$ (**2a**) show good agreement with the highest level ab initio calculated structures. Because the molecules have many degrees of flexibility, some of the experimental estimated standard deviations for the torsion angles are large, typically 2−3°.

The Ga atom in the gas-phase structure of **2a** is surrounded by two methyl groups as well as two oxygen atoms [O(4) from the direct bond with the alkoxide ligand and O(7) in the alkoxide chelate]. Similarly, the Ga atom in **1a** is surrounded by two methyl groups, as well as one oxygen O(4) and one nitrogen N(7) from the aminoalkoxide chelate. The Ga atoms in both **1a** and **2a** have, therefore, distorted tetrahedral arrangements, with the E(7)···Ga−C(2)/C(3)/O(4) angles in the range 81.6(10) to 107.9(19)° for **1a** and 81.5(3) to 108.7(5)° for **2a**.

The Ga···O distance in **2a** has been determined to be 2.160(20) Å in the gas phase. This can be compared to the Ga···O distance of 2.624(6) Å in the solid-state structure **2**.[24] Similarly, the Ga···N distance in **1a** was determined to be 2.332(11) Å in the gas phase, compared to the Ga···N distance of 2.471(4) Å in the solid-state structure **1**.[25] Thus there are relatively large differences between the distances observed in monomers and dimers, even taking into account the fundamental differences in physical meanings of the distances given by the two experimental methods that have been applied.

Such striking differences are also observed when we compare the calculated structures of monomers and dimers **1a**/**1** and **2a**/**2** in the gas phase. The calculated Ga···N distances for **1a**/**1** are 2.167 Å (monomer) and 2.332 Å (dimer), and the Ga···O distances for **2a** and **2** are 2.183 and 2.524 Å, respectively. We attribute this phenomenon to the fact that N is more basic than O. While there is a weak interaction in both monomers, it is weaker for O in **2** than for N in **1**.

The Ga−O(4) bond distances in **1a** and **2a** in the gas phase are 1.906(4) and 1.865(10) Å, respectively, which are similar in magnitude to the equatorial Ga−O bond lengths of 1.913(3) and 1.934(6) Å in the solid-state structures of **1** and **2**, but shorter than the axial Ga−O bond distances of 2.078(3) and 2.012(7) Å.[24,25] The average Ga−O bond length for tetrahedrally and octahedrally coordinated gallium atoms is 1.96 Å.[1,2,24,25] For the dimeric structures **1** and **2**, the equatorial bonds would be expected to be shorter and axial ones longer, based on hybridization effects alone, which is indeed observed. The shorter Ga−E distances observed in gas-phase **1a** and **2a** versus solid-state **1** and **2** are probably the result of monomer formation and the constraints of the chelating ring.[47]

The structure of $[Me_2Ga(O^tBu)]_2$ (**3**), which incorporates a monofunctional alkoxide, has also been investigated using GED. This was studied with a view to gaining an insight into the stabilizing effects of donor functionalized ligands and differences that may be encountered in the gas phase during a CVD process. While the structure of $[Me_2Ga(O^tBu)]_2$ obtained using X-ray crystallographic techniques has not been reported, spectroscopic data provide evidence that **3** is also dimeric in the solid state.[26] Furthermore, the single-crystal structures of analogous compounds such as $[^tBu_2Ga(O^tBu)]_2$[48] and $[H_2Ga(O^tBu)]_2$[49] have been described previously. Like **1** and **2**, these compounds are

dimeric, with planar centrosymmetric Ga_2O_2 rings at their centers.

Compound **3** is dimeric in the gas phase, with the two gallium cations and two alkoxide oxygen anions forming a centrosymmetric, planar four-membered Ga_2O_2 ring that is common to this type of compound in the solid state. Each monomeric unit is composed of one gallium cation, two methyl groups, and a *tert*-butyl alkoxide ligand. The crystallographic inversion center is located in the middle of the Ga_2O_2 ring. Each gallium atom in **3** thus adopts tetrahedral geometry. The bridging oxygen atoms of the Ga_2O_2 ring make up two of the corners of the gallium-centered tetrahedra, while the terminal methyl groups make up the remaining two corners. The Ga−C_{Me} bond lengths as determined by GED [all are 1.950(5) Å because of symmetry] suggest that the methyl groups are tightly bound to the gallium centers. The Ga−O bond length of 1.979(2) Å, reported here for the gas-phase structure of **3**, is comparable to Ga−O bond lengths in known solid-state structures; the average Ga−O bond length in $[H_2Ga(O^tBu)]_2$ is 1.905(9) Å,[48] and that in $[^tBu_2Ga(O^tBu)]_2$ is 1.990(2) Å.[49]

The gallium-centered tetrahedra are distorted, exhibiting bond angles that vary significantly from the approximately 109° seen in undistorted tetrahedra. The C−Ga−C bond angle (again symmetry dictates there is only one distinct angle) between the methyl groups on the gallium center is 122.2(16)°, and the O(3)−Ga(1)−O(2) bond angle is reported to be 81.5(2)°. Such large deviations from 109° are due, at least in part, to the steric constraints in the Ga_2O_2 ring in relation to the other substituents on the Ga atom, as is often the case with compounds of this type.[1,2] These bond angles are comparable with those of known compounds. For example, for $[H_2Ga(O^tBu)]_2$ the C−Ga−C and O−Ga−O angles are 116.0(1) and 78.6(5)° and for $[^tBu_2Ga(O^tBu)]_2$ they are 115.1(3) and 76.1(1)°.[48,49]

The existence of dative Ga···N/O bonds in structures **1a** and **2a**, as suggested by the experimentally determined structures, is confirmed by topological AIM[35] and ELF[38,39] analyses. The results of these analyses are given in Supporting Information, Tables S17−S20. The AIM results show that the Ga atom in structure **1a** is tetravalent (see Figure 6). The (3,−1) Ga···N bond critical point has been detected, the nomenclature
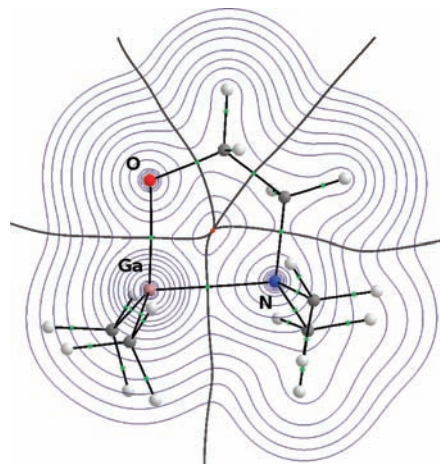

Figure 6. Superposition of the structure of molecule **1a** (solid lines linking atoms), relevant interatomic surfaces (lines perpendicular to the ring bonds), and a contour plot of the electron density in the GaON plane. The bond and ring critical point are marked by green and red dots, respectively.

showing that this is a minimum of the electron density with respect to the bond path linking Ga and N, and a maximum with respect to directions perpendicular to that vector. This is a prerequisite condition for the bond, as well as consistent topology of electron density [the presence of (3,+1) ring critical point].[50]

As might be expected, the dative bond formed between the Ga atom and the lone pair of electrons on the N atom is the weakest bond in molecule **1a**. The electron density at the (3,−1) bond critical point is very small (0.065 au), $\nabla\rho$ is positive (0.178 au), and the bond index (0.294) is much smaller that for the single covalent bonds present in the molecule. These data are consistent with the existence of a dative, strongly polarized bond. To estimate the strength of this bond we compared the total energy of cyclic structure **1a** with the energy of its most stable open conformer. The ZPE-corrected value is 85.8 kJ mol^{-1}, which is much less than a typical covalent single-bond enthalpy and is consistent with conclusions derived from AIM analysis.

Figure 7 shows the layout of bonding and free electron pairs defined using the ELF method. Each C−O, C−C, and C−N
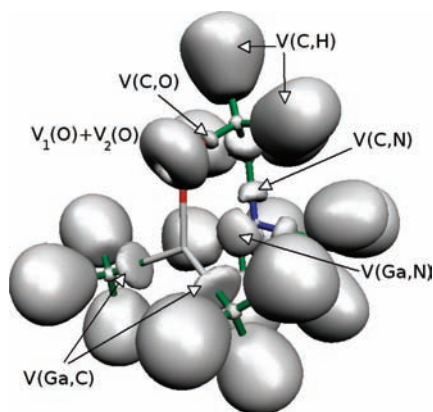
Figure 7. Electron localization domains of structure **1a**. The plot represents isosurfaces of the Electron Localization Function of value 0.8. V(X,Y) denotes a disynaptic basin representing an X−Y bond. V$_1$(O)+V$_2$(O) denotes two lone pairs of electrons on an oxygen atom.

bond is represented by a disynaptic basin [marked with V(X,Y)] in the space between two bonded atoms, which is a typical feature of a covalent bond. The electron populations of the valence disynaptic basins V(C,C) and V(C,N) are slightly below 2, which is the value expected for a single covalent bond.

The presence of the basin V(Ga,N) in **1a** confirms the dative bond linking atoms Ga and N. It can be seen from Figure 7 that the bond is formed by the donation to Ga of the lone pair of electrons on the N donor atom. This fact is shown quantitatively (see Supporting Information, Table S18) by the atomic contributions to the V(Ga,N) electron population. The total population of 2.21 e originates mainly from the N atom (2.08 e), while only a slight contribution comes from Ga (0.13 e). The bonding situation in **2a** is analogous to that in **1a**.

As described previously, the high symmetry of 3 forces chemical equivalence of all Ga−O bonds, which requires the Ga atom to have tetrahedral coordination. AIM calculations (see Supporting Information, Table S21) show that at the Ga−O bond critical point the electron density is small (0.083 au), and that there is a positive value of the Laplacian (0.369 au). The lack of any ELF disynaptic basins between Ga and O

atoms (Supporting Information, Figure S5) is consistent with the purely ionic nature of the Ga−O bonds in 3.

■ CONCLUSIONS

The full structural characterization of the monomeric forms of **1** and **2** in the gas phase using a combined electron diffraction and computational approach has been described. The structure of [Me$_2$Ga(O^{t}Bu)]$_2$, **3**, which retains its dimeric structure in the gas phase, is also reported. This difference in behavior gives us an insight into the driving force behind the transition from dimer to monomer for compounds **1** and **2**, which incorporate donor functionalized alkoxide ligands. Both **1a** and **2a** adopt structures in the gas phase that exhibit five-membered rings formed by a dative, strongly polarized bond between Ga and N or O, respectively. In **3** there is no possibility of a monomer structure stabilized by the formation of such a ring motif. Calculations show that the Ga−O bonds in **3** are ionic in nature.

Although dialkylalkoxygallanes incorporating donor functionalized ligands generally adopt dimeric structures in the solid state, in the gas phase monomers are likely to be present. Monomers are expected to exhibit enhanced volatility in comparison to oligomeric complexes, in which intermolecular solid-state interactions are likely to increase the enthalpy of vaporization. However, this work shows that the structure adopted in the solid state may differ from that in the gas phase and so compounds that appear unsuitable for CVD may in fact be feasible precursors. Overall, this study has provided information that can be used to aid the design of precursor molecules for a range of technologically important materials.

■ ASSOCIATED CONTENT

ⓢ Supporting Information

Additional details relating to the GED experiments (Table S1); details from the GED models and refinements (Tables S2−S4); amplitudes of vibration and curvilinear distance corrections from the GED refinements (Tables S5−S7); least-squares correlation matrices (Tables S8−S10); final GED coordinates and highest-level calculated coordinates and energies (Tables S11−S16); results of AIM and ELF calculations (Tables S17−S21); plot of Gibbs free energy (ΔG) and entropy (ΔS) for dimerization of [Me$_2$Ga(OCH$_2$CH$_2$NMe$_2$)] (**1a**) (Figure S1); molecular-scattering intensity curves (Figures S2−S4); pictorial representation of the ELF results for **3** (Figure S5). This material is available free of charge via the Internet at http://pubs.acs.org.

■ AUTHOR INFORMATION

Corresponding Author
*E-mail: derek.wann@ed.ac.uk (D.A.W.), abil@elrond.chem. uni.wroc.pl (A.B.), c.j.carmalt@ucl.ac.uk (C.J.C.).
Notes
The authors declare no competing financial interest.

■ ACKNOWLEDGMENTS

■ REFERENCES

(1) Carmalt, C. J.; King, S. J. *Coord. Chem. Rev.* **2006**, *250*, 682.

(2) Bloor, L.; Pugh, D.; Carmalt, C. J. *Coord. Chem. Rev.* **2011**, *255*, 1293.

(3) Coates, G. E.; Hayter, R. G. *J. Chem. Soc.* **1953**, 2519.

(4) Schwering, H.-U.; Jungk, E.; Weidlein, J. *J. Organomet. Chem.* **1975**, *91*, C4.

(5) Basharat, S.; Carmalt, C. J.; King, S. J.; Peters, E. S.; Tocher, D. A. *Dalton Trans.* **2004**, 3475.

(6) Miinea, L.; Suh, S.; Bott, S. G.; Liu, J.-R.; Chu, W.-K.; Hoffman, D. M. *J. Mater. Chem.* **1999**, *9*, 929.

(7) Valet, M.; Hoffman, D. M. *Chem. Mater.* **2001**, *13*, 2135.

(8) Basharat, S.; Carmalt, C. J.; Barnett, S. A.; Tocher, D. A.; Davies, H. O. *J. Organomet. Chem.* **2008**, *693*, 1787.

(9) Knapp, C. E.; Pemberton, L.; Carmalt, C. J.; Pugh, D.; McMillan, P. F.; Barnett, S. A.; Tocher, D. A. *Main Group Chem.* **2010**, *9*, 31. Knapp, C. E.; Pugh, D.; McMillan, P. F.; Parkin, I. P.; Carmalt, C. J. *Inorg. Chem.* **2011**, *50*, 9491.

(10) Basharat, S.; Carmalt, C. J.; Binions, R.; Palgrave, R.; Parkin, I. P. *Dalton Trans.* **2008**, 591.

(11) Basharat, S.; Knapp, C. E.; Carmalt, C. J.; Barnett, S. A.; Tocher, D. A. *New J. Chem.* **2008**, *32*, 1513.

(12) Suh, S.; Hoffman, D. M. *J. Am. Chem. Soc.* **2000**, *122*, 9396.

(13) Basharat, S.; Carmalt, C. J.; Barnett, S. A.; Tocher, D. A.; Davies, H. O. *Inorg. Chem.* **2007**, *46*, 9473.

(14) Knapp, C. E.; Hyett, G.; Parkin, I. P.; Carmalt, C. J. *Chem. Mater.* **2011**, *23*, 1719.

(15) Knapp, C. E.; Kafizas, A.; Parkin, I. P.; Carmalt, C. J. *J. Mater. Chem.* **2011**, *21*, 12644.

(16) Fleischer, M.; Meixner, H. *Sens. Actuators, B* **1993**, *13*, 259.

(17) Binions, R.; Carmalt, C. J.; Parkin, I. P. *Meas. Sci. Technol.* **2007**, *18*, 190.

(18) Knapp, C. E.; Carmalt, C. J.; McMillan, P. F.; Wann, D. A.; Robertson, H. E.; Rankin, D. W. H. *Dalton Trans.* **2008**, 6880.

(19) Davis, M. J.; Pemble, M. E. *J. Phys.-Paris IV* **1999**, *9*, 49.

(20) Vemardou, D.; Pemble, M. E.; Sheel, D. W. *Thin Solid Films* **2007**, *515*, 8768.

(21) Vernardou, D.; Pemble, M. E.; Sheel, D. W. *Thin Solid Films* **2008**, *516*, 4502.

(22) Holdsworth, R. J.; Martin, P. A.; Raisbeck, D.; Rivero, J.; Sanders, H. E.; Sheel, D. W.; Pemble, M. E. *Chem. Vap. Deposition* **2001**, *7*, 39.

(23) Gould, B. J.; Povey, I. M.; Pemble, M. E.; Flavell, W. R. *J. Mater. Chem.* **1994**, *4*, 1815.

(24) Schumann, H.; Frick, M.; Heymer, B.; Girgsdies, F. *J. Organomet. Chem.* **1996**, *512*, 117.

(25) Rettig, S. J.; Storr, A.; Trotter, J. *Can. J. Chem.* **1975**, *53*, 58.

(26) Schmidbaur, H. *Angew. Chem., Int. Ed. Engl.* **1965**, *4*, 152.

(27) National Service for Computational Chemistry Software (NSCCS). URL http://www.nsccs.ac.uk

(28) Frisch, M. J.; Trucks, G. W.; Schlegel, H. B.; Scuseria, G. E.; Robb, M. A.; Cheeseman, J. R.; Montgomery, J. A., Jr.; Vreven, T.; Kudin, K. N.; Burant, J. C.; Millam, J. M.; Iyengar, S. S.; Tomasi, J.; Barone, V.; Mennucci, B.; Cossi, M.; Scalmani, G.; Rega, N.; Petersson, G. A.; Nakatsuji, H.; Hada, M.; Ehara, M.; Toyota, K.; Fukuda, R.; Hasegawa, J.; Ishida, M.; Nakajima, T.; Honda, Y.; Kitao, O.; Nakai, H.; Klene, M.; Li, X.; Knox, J. E.; Hratchian, H. P.; Cross, J. B.; Adamo, C.; Jaramillo, J.; Gomperts, R.; Stratmann, R. E.; Yazyev, O.; Austin, A. J.; Cammi, R.; Pomelli, C.; Ochterski, J. W.; Ayala, P. Y.; Morokuma, K.; Voth, G. A.; Salvador, P.; Dannenberg, J. J.; Zakrzewski, V. G.; Dapprich, S.; Daniels, A. D.; Strain, M. C.; Farkas, O.; Malick, D. K.; Rabuck, A. D.; Raghavachari, K.; Foresman, J. B.; Ortiz, J. V.; Cui, Q.; Baboul, A. G.; Clifford, S.; Cioslowski, J.; Stefanov, B. B.; Liu, G.; Liashenko, A.; Piskorz, P.; Komaromi, I.; Martin, R. L.; Fox, D. J.; Keith, T.; Al-Laham, M. A.; Peng, C. Y.; Nanayakkara, A.; Challacombe, M.; Gill, P. M. W.; Johnson, B.; Chen, W.; Wong, M. W.; Gonzalez, C.; Pople, J. A. *Gaussian 03*, revision C.02; Gaussian, Inc.: Wallingford, CT, 2004.

(29) Binkley, J. S.; Pople, J. A.; Hehre, W. J. *J. Am. Chem. Soc.* **1980**, *102*, 939. Gordon, M. S.; Binkley, J. S.; Pople, J. A.; Pietro, W. J.; Hehre, W. J. *J. Am. Chem. Soc.* **1982**, *104*, 2797. Pietro, W. J.; Francl, M. M.; Hehre, W. J.; DeFrees, D. J.; Pople, J. A.; Binkley, J. S. *J. Am. Chem. Soc.* **1982**, *104*, 5039.

(30) Hehre, W. J.; Ditchfield, R.; Pople, J. A. *J. Chem. Phys.* **1972**, *56*, 2257. Hariharan, P. C.; Pople, J. A. *Theor. Chim. Acta* **1973**, *28*, 213. Gordon, M. S. *Chem. Phys. Lett.* **1980**, *76*, 163.

(31) Møller, C.; Plesset, M. S. *Phys. Rev.* **1934**, *46*, 618.

(32) Krishnan, R.; Binkley, J. S.; Seeger, R.; Pople, J. A. *J. Chem. Phys.* **1980**, *72*, 650. McLean, A. D.; Chandler, G. S. *J. Chem. Phys.* **1980**, *72*, 5639.

(33) Sipachev, V. A. *J. Mol. Struct. (THEOCHEM)* **1985**, *121*, 143. Sipachev, V. A. *J. Mol. Struct.* **2001**, *567*, 67.

(34) Becke, A. D. *J. Chem. Phys.* **1993**, *98*, 5648. Lee, C.; Yang, W.; Parr, R. G. *Phys. Rev. B* **1992**, *37*, 785.

(35) Bader, R. F. W. *Atoms in Molecules: A Quantum Theory*; Oxford University Press: Oxford, U.K., 1994; Bader, R. F. W. *Chem. Rev.* **1991**, *91*, 893.

(36) Bader, R. F. W. *J. Phys. Chem. A* **1998**, *102*, 7314.

(37) Keith, T. A. *AIMAll* (version 11.03.14); TK Gristmill Software: Overland Park, KS, 2011.

(38) Becke, A. D.; Edgecombe, K. E. *J. Chem. Phys.* **1990**, *92*, 5397.

(39) Silvi, B.; Savin, A. *Nature* **1994**, *371*, 683. Savin, A.; Nesper, R.; Wengert, S.; Fässler, T. *Angew. Chem., Int. Ed. Engl.* **1997**, *36*, 1808.

(40) Noury, S.; Krokidis, X.; Fuster, F.; Silvi, B. *Comput. Chem.* **1999**, *23*, 597.

(41) Huntley, C. M.; Laurenson, G. S.; Rankin, D. W. H. *J. Chem. Soc., Dalton Trans.* **1980**, 954.

(42) Schirlin, J. T. Ph.D. Thesis, University of Edinburgh, Edinburgh, U.K., 2004.

(43) Fleischer, H.; Wann, D. A.; Hinchley, S. L.; Borisenko, K. B.; Lewis, J. R.; Mawhorter, R. J.; Robertson, H. E.; Rankin, D. W. H. *Dalton Trans.* **2005**, 3221.

(44) Hinchley, S. L.; Robertson, H. E.; Borisenko, K. B.; Turner, A. R.; Johnston, B. F.; Rankin, D. W. H.; Ahmadian, M.; Jones., J. N.; Cowley, A. H. *Dalton Trans.* **2004**, 2469.

(45) Ross, A. W.; Fink, M.; Hilderbrandt, R. In *International Tables for Crystallography*; Wilson, A. J. C., Ed.; Kluwer Academic Publishers: Dordrecht, The Netherlands, 1992; Vol. C, p 245.

(46) Blake, A. J.; Brain, P. T.; McNab, H.; Miller, J.; Morrison, C. A.; Parsons, S.; Rankin, D. W. H.; Robertson, H. E.; Smart, B. A. *J. Phys. Chem.* **1996**, *100*, 12280. Brain, P. T.; Morrison, C. A.; Parsons, S.; Rankin, D. W. H. *J. Chem. Soc., Dalton Trans.* **1996**, 4589. Mitzel, N. W.; Rankin, D. W. H. *Dalton Trans.* **2003**, 3650.

(47) Chi, Y.; Chou, T.-Y.; Wang, Y.-J.; Huang, S.-F.; Carty, A. J.; Scoles, L.; Udachin, K. A.; Peng, S.-M.; Lee, G.-H. *Organometallics* **2004**, *23*, 95.

(48) Power, M. B.; Cleaver, W. M.; Apblett, A. W.; Barron, A. R.; Ziller, J. W. *Polyhedron* **1992**, *11*, 477.

(49) Veith, M.; Faber, S.; Wolfanger, H.; Huch, V. *Chem. Ber.* **1996**, *129*, 381.

(50) Bader, R. F. W.; Nguyen-Danf, T. T.; Tal, Y. *Rep. Prog. Phys.* **1981**, *44*, 893.